Characterization of the molecular parameters determining charge transport in anthradithiophene

O. Kwon, V. Coropceanu, N. E. Gruhn, J. C. Durivage, J. G. Laquindanum et al.

Citation: J. Chem. Phys. **120**, 8186 (2004); doi: 10.1063/1.1689636
View online: http://dx.doi.org/10.1063/1.1689636
View Table of Contents: http://jcp.aip.org/resource/1/JCPSA6/v120/i17
Published by the American Institute of Physics.

Characterization of the molecular parameters determining charge transport in anthradithiophene

O. Kwon and V. Coropceanu
School of Chemistry and Biochemistry, Georgia Institute of Technology, Atlanta, Georgia 30332-0400

N. E. Gruhn and J. C. Durivage
Department of Chemistry, The University of Arizona, Tucson, Arizona 85721-0041

J. G. Laquindanum and H. E. Katz
AT&T Bell Laboratories, Lucent Technologies, Murray Hill, New Jersey 07974-0636

J. Cornil
Laboratory for Chemistry of Novel Materials, Center for Research on Molecular Electronics and Photonics, University of Mons-Hainaut, Place du Parc 20, B-7000 Mons, Belgium and School of Chemistry and Biochemistry, Georgia Institute of Technology, Atlanta, Georgia 30332-0400

J. L. Brédas
School of Chemistry and Biochemistry, Georgia Institute of Technology, Atlanta, Georgia 30332-0400 and Laboratory for Chemistry of Novel Materials, Center for Research on Molecular Electronics and Photonics, University of Mons-Hainaut, Place du Parc 20, B-7000 Mons, Belgium

(Received 18 December 2003; accepted 3 February 2004)

The molecular parameters that govern charge transport in anthradithiophene (ADT) are studied by a joint experimental/theoretical approach involving high-resolution gas-phase photoelectron spectroscopy and quantum-mechanical methods. The hole reorganization energy of ADT has been determined by an analysis of the vibrational structure of the lowest ionization band in the gas-phase photoelectron spectrum as well as by density-functional theory calculations. In addition, various dimers and clusters of ADT molecules have been considered in order to understand the effect of molecular packing on the hole and electron intermolecular transfer integrals. The results indicate that the intrinsic electronic structure, the relevant intramolecular vibrational modes, and the intermolecular interactions in ADT are very similar to those in pentacene. © *2004 American Institute of Physics.* [DOI: 10.1063/1.1689636]

I. INTRODUCTION

Organic π-conjugated materials are being increasingly used as active elements in optoelectronic devices such as field-effect transistors (FET's),[1–8] light-emitting diodes (LED's),[9–12] or photovoltaic and solar cells.[13–16] Organic materials offer the advantages of easy fabrication, mechanical flexibility, and low cost. A number of organic materials have now demonstrated useful FET performance, which can be characterized by their field mobilities and on/off current ratios. For instance, the mobility of pentacene reaches 5 $cm^2/V\,s$ and exceeds that in amorphous silicon FET's.[17–20]

Despite its adequate charge transport properties, pentacene suffers from oxidative instability and insolubility.[21] In addition, the herringbone packing of pentacene molecules in the solid state does not provide for optimal intermolecular π-orbital overlap, which is a critical factor impacting the intrinsic carrier mobility.[22] Many attempts have been made to improve the stability and charge transport properties of pentacene by substrate modification or functionalization of the molecular structure.[23–27] Anthony *et al.* synthesized pentacene derivatives showing a significant amount of π stacking in the crystal;[24–25] however, recent density-functional theory (DFT) calculations indicate that the reorganization energies for these functionalized pentacenes are about 50% higher than in pentacene itself.[28] Recently, Meng *et al.* prepared single crystals of a pentacene derivative where the four terminal hydrogens are substituted by methyl groups;[26] the crystal structure and calculated reorganization energy of this derivative are found to be very similar to those of pristine pentacene.

Another strategy is to design isostructural analogues of pentacene such as anthradithiophene (ADT) and dihydrodiazapentacene.[27,29,30] Katz and co-workers[29,30] have recently shown that ADT, see sketch below, and its alkyl derivatives exhibit a mobility (0.06–0.15 $cm^2/V\,s$) approaching that of pentacene.

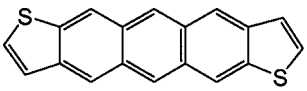

anti ADT

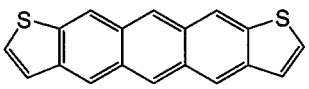

syn ADT

In addition, the α carbons of the terminal thiophene rings in ADT can be substituted to enhance solubility, morphology, and adhesion for processing. It is therefore of interest to evaluate the molecular parameters affecting the charge transport properties in ADT and to compare them to those in pentacene. Here, we report a detailed quantum-mechanical characterization of the charge transport properties of ADT together with an analysis of its gas-phase ionization spectrum.

II. EXPERIMENT

ADT has been synthesized as mixtures of anti and syn isomers as previously described.[30] The gas-phase photoelectron spectrum of ADT was collected using the instrument and experimental procedures reported in more detail elsewhere.[31] The sample sublimed at 220–280 °C with no evidence of contaminants present in the gas phase during data collection. The instrument resolution during data collection was better than 35 meV (measured using the full width at half height for the $^2P_{3/2}$ ionization of Ar).

III. THEORETICAL METHODOLOGY

We first recall that the main parameters governing charge transport at the molecular level are the electronic couplings (transfer integrals, t) between adjacent oligomers and the reorganization energies due to hole-vibration or electron-vibration interactions.[22,32,33] In perfectly ordered materials at very low temperature, provided the bandwidths are significant, charge transport can be described in terms of a bandlike regime. In this case, the total valence and conduction bandwidths resulting from the interaction of the HOMO (highest occupied molecular orbital) and LUMO (lowest unoccupied molecular orbital) levels of the individual units determine the hole and electron mobilities, respectively. In a tight-binding model, the total valence and conduction bandwidths of an infinite one-dimensional stack is equal to four times the intermolecular transfer integrals.

At high temperature, when the motion of the carriers can be modeled by sequences of uncorrelated hops, the mobility can be expressed as[34–36]

$$\mu = \frac{ea^2}{k_B T} k_{\mathrm{ET}}. \tag{1}$$

Here, k_B denotes the Boltzmann constant, T the temperature, e the electronic charge, a the spacing between the molecules, and k_{ET} the hopping probability per unit time (electron-transfer rate). In the context of semiclassical electron-transfer (ET) theory and extensions thereof,[37–39] there are two major parameters that determine the self-exchange ET rate and ultimately the charge mobility: (i) the intermolecular transfer integral t, that (as in the case of the bandlike regime) should be maximized; and (ii) the reorganization energy λ, which needs to be small for efficient transport. The reorganization energy includes the molecular geometry modifications that occur when an electron is added to or removed from a molecule (inner reorganization) as well as the modifications in the surrounding medium due to polarization effects (outer reorganization). We note that the weakness of the van der Waals interactions among organic molecules makes the separation of the reorganization energy into inner and outer molecular contributions reasonable, even in the case of molecular crystals. In the high-temperature limit, the rate constant is given by[40]

$$k_{\mathrm{ET}} = A \cdot \exp\left[-\frac{(\lambda - 2t)^2}{4\lambda k_B T} \right]. \tag{2}$$

Prefactor A depends on the strength of the electronic coupling (i.e., the transfer integrals): in the case of weak coupling (nonadiabatic ET regime), $A \approx t^2$; in the case of strong coupling (adiabatic ET regime), $A = \nu_n$, where ν_n is the frequency for nuclear motion along the reaction coordinate.

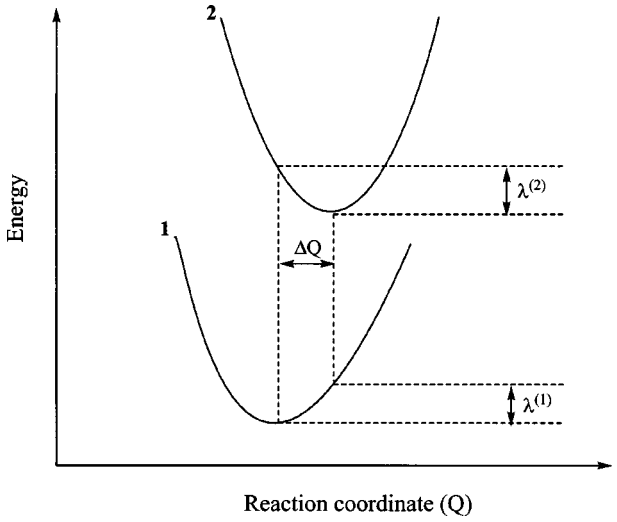

FIG. 1. Schematic diagram of general adiabatic energy surfaces corresponding to the ionization process ΔQ is a normal-mode displacement and $\lambda^{(1)}$ and $\lambda^{(2)}$ are relaxation energies.

Here, we focus on the intramolecular reorganization energy and its vibrational mode description. The intramolecular reorganization energy for self-exchange consists of two terms corresponding to the geometry relaxation energies ($\lambda_{\mathrm{rel}}^{(1)}$ and $\lambda_{\mathrm{rel}}^{(2)}$) when going from the neutral-state geometry to the charged-state geometry and vice versa, see Fig. 1.[35,36] The λ terms were evaluated in two ways: (i) they were computed directly from the adiabatic potential-energy surfaces of neutral/cation and neutral/anion species using the procedure outlined in Ref. 41; (ii) they were obtained on the basis of a normal-mode analysis, which provides as well the partition of the total relaxation (reorganization) energy into the contributions from each vibrational mode:[38,42,43]

$$\lambda_{\mathrm{rel}} = \sum \lambda_i = \sum \frac{1}{2} k_i \Delta Q_i^2, \tag{3}$$

where ΔQ_i represents the displacement along normal mode Q_i between the equilibrium geometries of the neutral and charged molecules; k_i is the corresponding force constant.

The geometries of the neutral, cation, and anion species of both anti and syn ADT isomers were optimized at the DFT level[44,45] by using the B3LYP functionals[46] with the 6-31G** basis set,[47] and the vibrational frequencies and normal modes were evaluated. All DFT calculations were performed with the GAUSSIAN98 program.[48]

The transfer integrals quantify the electronic coupling between two interacting oligomers (M_a and M_b) and are defined by the matrix element $t = \langle \Psi_1 | V | \Psi_2 \rangle$, where the operator V describes the intermolecular interactions and Ψ_1 and Ψ_2 are the wave functions corresponding to the two charge localized states $M_a^- - M_b$ and $M_a - M_b^-$ [or $M_a^+ - M_b$ and $M_a - M_b^+$], respectively.[49,50] It is, however, possible to obtain a simple and reliable estimate by applying Koopmans' theorem.[51] In this context, the absolute value of the transfer integral for electron [hole] transfer is approxi-

mated by the energy difference, $t=(\varepsilon_{L+1[H]}-\varepsilon_{L[H-1]})/2$, where $\varepsilon_{L[H]}$ and $\varepsilon_{L+1[H-1]}$ are the energies of LUMO and LUMO+1 [HOMO and HOMO−1] orbitals taken from the closed-shell configuration of the neutral state of a dimer (M_a-M_b).[49,50] The sign of t can be obtained from the symmetry of the corresponding frontier orbitals of a dimer; t is negative if LUMO [HOMO] of the dimer (M_a-M_b) is symmetric (i.e., represents a bonding combination of monomer LUMO's [HOMO's]) and positive if LUMO [HOMO] is antisymmetric (antibonding combination of monomer LUMO [HOMO]'s).[50]

Here, we evaluate the transfer integrals obtained by Koopmans' theorem from the electronic structures calculated at the semiempirical INDO level.[52,53] The INDO method has been successful in describing the electronic structures of isolated and interacting conjugated molecules and provides results in excellent agreement with corresponding experimental data[33,54–56] and theoretical *ab initio* results.[57] We have analyzed the way the transfer integrals are affected by the relative orientations of the molecules in the solid state. In the absence of crystal-structure data for ADT, we have investigated: (i) the influence of intermolecular separation by considering cofacial dimers (with respect to the thiophene rings in ADT) and changing the distance between the molecular planes in the range 3.5–5.0 Å; (ii) for a fixed intermolecular distance of 4.0 Å in a cofacial dimer, the impact of lateral displacements of one of the molecules, along both the long and short molecular axes; (iii) the evolution of the transfer integrals as a function of the number of molecules in a one-dimensional cofacial π stack (that is, as a function of cluster size). The results are compared to those obtained in similar conditions for pentacene.

IV. RESULTS AND DISCUSSION

The experimental gas-phase ultraviolet photoemission spectroscopy (UPS) spectrum of ADT is shown in Fig. 2 together with that of pentacene;[28] the two spectra are very similar. The first ionization of ADT has a vertical energy of 6.699±0.001 eV vs 6.589±0.001 eV for pentacene and is well separated from the other ionizations of the molecule. Several ionizations show partially resolved vibrational fine structure. A closeup of the lowest binding energy peak associated to the HOMO level is shown in Fig. 3. As is the case in pentacene,[28] the first ionization clearly exhibits a high-frequency progression of about 1400 cm^{-1} that lies in the region expected for C–C stretching modes. The line shape of the lowest UPS band is directly related to the geometry relaxation energy, $\lambda_{rel}^{(1)}$, calculated when going from the neutral ground-state geometry to the cation optimal geometry; $\lambda_{rel}^{(1)}$ closely corresponds to one-half the vibrational reorganization energy for intramolecular hole transfer.[28] The similarity in the shape of the first ionization peak in ADT and pentacene points to the fact that the reorganization energy of ADT is as small as in pentacene, as further supported by the DFT-B3LYP calculations.

The B3LYP/6-31G**-optimized geometries of the anti and syn isomers of ADT are shown together with that of pentacene in Fig. 4. The anti and syn isomers are calculated

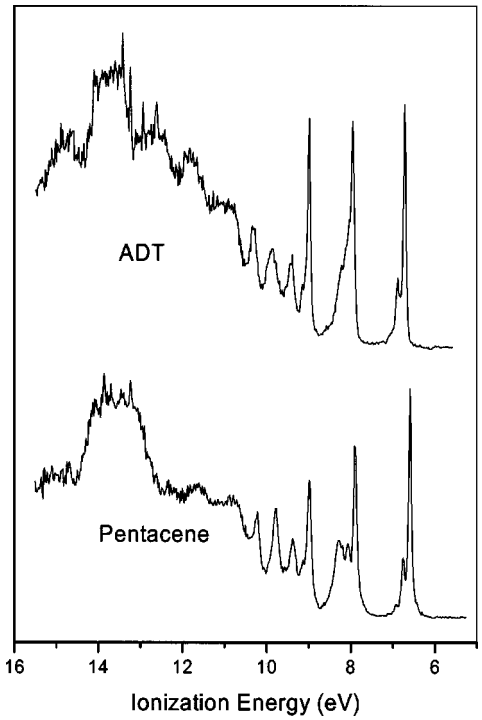

FIG. 2. Gas-phase photoelectron spectra of ADT (top) and pentacene.

to be nearly isoenergetic: the anti isomer is very slightly more stable than the syn isomer by 0.02 kcal/mol. The calculated C–C bond distances in the ADT isomers show a reduced bond-length alternation compared to pentacene. The DFT-B3LYP adiabatic ionization potential (IP) of ADT is estimated to be 6.15 eV for both anti and syn isomers, which is comparable to the value obtained for pentacene (5.93 eV) at the same level of theory; the calculated IP's of both ADT and pentacene are lower than the experimental values by about 0.6 eV. The fact that IP is slightly higher in ADT than in pentacene is expected from the replacement of the two C═C bonds of pentacene with the slightly more electronegative sulfur atoms present in ADT.[58]

The degree of geometry relaxations calculated when going from the neutral to the cation or anion states is similar to

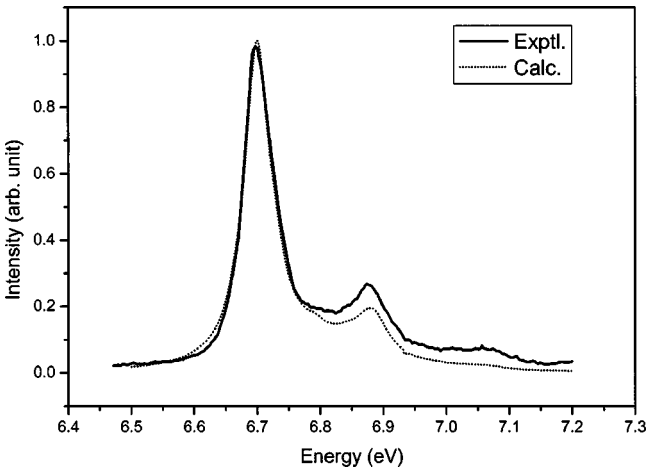

FIG. 3. High-resolution closeup of the first ionization of ADT.

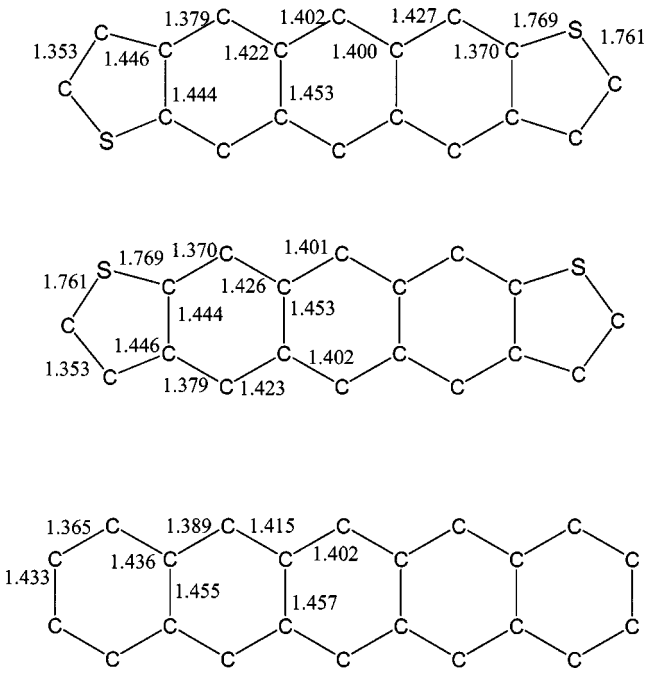

FIG. 4. Optimized bond distances (in Å) of the ADT isomers and pentacene at the B3LYP/6-31G** level. Only the symmetry-unique values are shown (anti ADT: C_{2h} symmetry, syn ADT: C_{2v} symmetry, pentacene: D_{2h} symmetry).

those observed in pentacene. The C–C bond distances change by about 0.01 Å in both isomers of ADT (0.01 Å for pentacene); for both isomers, the change in the C–S bond distances when going from the neutral molecule to the cation (0.02 Å) is much larger than that calculated upon reduction (0.004 Å). This is easily understood from an analysis of the shape of the ADT frontier orbitals (see Fig. 5); the HOMO level presents an antibonding character between the carbon and sulfur atoms, which leads to a shortening of the C–S bonds when one electron is removed; in contrast, the sulfur atoms do not contribute to the LUMO level, which results in small changes in the C–S bond distances when one electron is added. Comparison of the frontier orbitals in ADT and pentacene indicates that the bonding–antibonding pattern of the orbitals is nearly the same (especially in the central anthracene unit), see Fig. 5; thus modifying pentacene by introducing thiophene rings hardly changes the electronic characteristics. This has also been found in the previous study of anthracene and naphthothiophenes (isoelectronic with anthracene).[58]

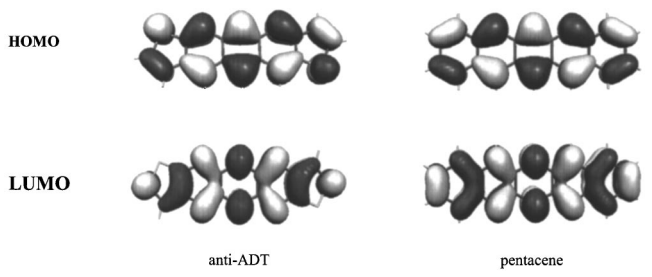

FIG. 5. Bonding–antibonding pattern of the HOMO and LUMO of ADT and pentacene at the B3LYP/6-31G** level.

TABLE I. DFT-B3LYP estimates of the relaxation energies $\lambda_{rel}^{(1)}$ and $\lambda_{rel}^{(2)}$ and reorganization energies λ (in eV), associated to hole- and electron-vibrational couplings in ADT and pentacene.

		Hole transfer			Electron transfer		
Molecule	Method	$\lambda_{rel}^{(1)}$	$\lambda_{rel}^{(2)}$	λ	$\lambda_{rel}^{(1)}$	$\lambda_{rel}^{(2)}$	λ
ADT (anti)	AP[a]	0.048	0.048	0.096	0.081	0.080	0.161
	NM[b]	0.047	0.045	0.092	0.083	0.084	0.167
ADT (syn)	AP[a]	0.047	0.047	0.094	0.080	0.079	0.159
	NM[b]	0.047	0.046	0.093	0.088	0.080	0.168
Pentacene	AP[a]	0.048	0.049	0.097	0.066	0.066	0.132
	NM[b]	0.051	0.048	0.099	0.064	0.068	0.132

[a]Values calculated from the adiabatic potential (AP) surfaces of the neutral and charged species.
[b]Values obtained from a normal-mode (NM) analysis.

Table I collects the theoretical estimates of the relaxation energies of the charged species from the calculated adiabatic potentials (AP's) and from a normal-mode (NM) analysis. The reorganization energies (λ) obtained from both AP and NM approaches are in excellent agreement. The two components $\lambda_{rel}^{(1)}$ and $\lambda_{rel}^{(2)}$ of the total reorganization energy (λ) are nearly identical, as also observed for other systems.[32,41] The reorganization energies calculated for both ADT isomers are very similar and are larger by 40–45% for the anion; this is also the case in pentacene for which λ in the anion is 25–27% larger than that in the cation. The larger reorganization energy for the anion is rationalized by the fact that the geometry modifications upon reduction are more pronounced than upon oxidation. Comparison of the reorganization energies suggests that ADT behaves much like pentacene in terms of hole- and electron-vibrational coupling.

The partition of the relaxation energies of ADT isomers and pentacene into the contributions of each normal mode (considering only symmetric modes) is reported in Table II. The main contributions to the relaxation energy for the cationic species originate in vibrational modes in the range 760–1600 cm^{-1} for both ADT isomers, while in the pentacene cation they come from vibrational modes in the range 1200–1600 cm^{-1}. The vibrational modes yielding the largest contribution to the relaxation energies for the cationic species are at 1585 cm^{-1} (anti ADT), 1584 cm^{-1} (syn ADT), and 1560 cm^{-1} (pentacene); they all correspond to in-plane C–C stretching modes, thus explaining the similarity of the vibrational structure observed in the gas-phase photoelectron spectra of ADT and pentacene shown in Fig. 2. The vibrational modes around 800 cm^{-1} that contribute in ADT are characterized by in-plane C–S stretching modes.

For the anions of both ADT isomers, there is a strong coupling with a low-energy vibration, around 250 cm^{-1} (at 268 and 245 cm^{-1} in the anti and syn isomers, respectively), accounting for about 20% of the total relaxation energy; this vibration corresponds to in-plane C–C stretching mostly localized within the terminal thiophene rings. In pentacene, a significant contribution (28%) to the relaxation energies comes from a normal mode at 263 cm^{-1} also related to in-plane C–C stretching within the terminal benzene rings. This relatively strong interaction with a low-frequency mode in the anionic state, which is absent in the cationic state, has

TABLE II. Vibrational frequencies ω (cm^{-1}) and relaxation energies λ_{rel} (meV and cm^{-1} in parentheses) associated to the totally symmetric vibrations of ADT and pentacene in their singly oxidized and reduced states.

ADT											
anti				syn				Pentacene			
cation		anion		cation		anion		cation		anion	
ω	λ_{rel}	ω	λ_{rel}	ω	λ_{rel}	ω	λ_{rel}	ω	λ_{rel}	ω	λ_{rel}
222	2(16)	220	7 (56)	123	0 (0)	122	0 (0)	263	1 (8)	263	18(145)
270	1 (8)	268	13(105)	246	3 (24)	245	20(161)	613	0 (0)	616	3 (24)
431	0 (0)	435	1 (8)	354	0 (0)	350	2 (16)	636	0 (0)	638	0 (0)
523	0 (0)	524	0 (0)	561	1 (8)	550	3 (24)	765	0 (0)	756	2 (16)
619	1 (8)	614	0 (0)	624	0 (0)	624	1 (8)	807	0 (0)	800	1 (8)
650	2(16)	643	4 (32)	684	0 (0)	678	1 (8)	1046	0 (0)	1041	0 (0)
689	0 (0)	681	0 (0)	765	4 (32)	752	0 (0)	1200	3 (24)	1176	1 (8)
798	4(32)	784	2 (16)	825	1 (8)	814	4 (32)	1227	8 (65)	1219	5 (40)
853	1 (8)	847	7 (56)	848	0 (0)	838	5 (40)	1338	1 (8)	1325	1 (8)
1052	2(32)	1029	1 (8)	1031	2 (16)	1008	1 (8)	1426	1 (8)	1409	1 (8)
1116	1 (8)	1098	2 (16)	1117	0 (0)	1099	1 (8)	1441	18(145)	1427	22(177)
1197	4(32)	1178	4 (32)	1202	5 (40)	1187	3 (24)	1515	0 (0)	1511	1 (8)
1224	2(16)	1206	1 (8)	1277	1 (8)	1259	0 (0)	1560	11 (89)	1548	4 (32)
1306	0 (0)	1288	0 (0)	1313	0 (0)	1296	2 (16)	1590	8 (65)	1580	1 (8)
1322	0 (0)	1302	1 (8)	1354	1 (8)	1332	1 (8)	3192	0 (0)	3141	1 (8)
1378	2(16)	1359	4 (32)	1439	9 (73)	1416	17(137)	3196	0 (0)	3147	1 (8)
1443	4(32)	1418	10 (81)	1451	1 (8)	1427	1 (8)	3202	0 (0)	3152	1 (8)
1471	5(40)	1458	5 (40)	1487	2 (16)	1475	3 (24)	3224	0 (0)	3179	1 (8)
1519	0 (0)	1534	0 (0)	1536	0 (0)	1544	2 (16)				
1576	5(40)	1548	1 (8)	1584	17(137)	1580	18(145)				
1585	11(89)	1574	15(121)	1627	0 (0)	1614	2 (16)				
1609	2(16)	1596	4 (32)	3191	0 (0)	3141	0 (0)				
3237	0 (0)	3187	1 (8)	3237	0 (0)	3187	1 (8)				

also been found in other oligoacenes and their derivatives.[59–61]

The normal-mode analysis has been further exploited to simulate the shape of the first ionization peak in the UPS spectrum. In the framework of the Born–Oppenheimer and Franck–Condon (FC) approximations, the shape of the ionization band is governed by the overlap (Franck–Condon integral), $\mathrm{FCI}(m,n)=\langle\Phi_m(Q)|\Phi_n(Q)\rangle$, of the vibrational functions; here, $\Phi_m(Q)$ and $\Phi_n(Q)$ correspond to a mode associated to the neutral and cationic states, respectively. When Duschinsky mixing[62,63] is neglected, the relative intensity of a multidimensional vibrational transition, involving p vibrational modes, is obtained as a simple product of one-dimensional FC integrals:[64,65]

$$I(m_1,n_1,\ldots,m_p,n_p)=\prod_{i=1}^{p}\mathrm{FCI}(m_i,n_i)^2\exp\left\{\frac{-\hbar m_i\omega_i}{k_BT}\right\}, \tag{4}$$

$$\mathrm{FCI}(m,n)^2=\exp\{-S\}S^{(n-m)}\frac{m!}{n!}[L_m^{(n-m)}(S)]^2, \tag{5}$$

where m_i and n_i are the initial and final vibrational quantum numbers of the mode ω_i while the $S_i=\lambda_i/\hbar\omega_i$ terms are the Huang–Rhys factors (hole-vibrational constants) and $L_n^{(m)}$ is a Laguerre polynomial.[64]

The results of the simulation are shown in Fig. 3 for ADT. The positions of the peaks are very well reproduced, although the intensity of the feature around 6.9 eV is underestimated compared to the experimental one. The overall agreement between the simulated and experimental spectra increases the confidence in the reliability of DFT-derived vibronic constants and relaxation energies. The simulation also points to the role of multimode effects to get a better understanding of the UPS data and supports the DFT estimate of the reorganization energy in ADT.

We now turn to a discussion of the transfer integrals. The DFT-optimized geometries have been used to build dimers and clusters in a specific way, from which single-point calculations have been performed at the INDO level to calculate the intermolecular transfer integrals and understand the influence of the relative positions of the molecules (see Fig. 6) and the size of the clusters on the electronic splittings. A cofacial dimer where the two molecules are exactly superimposed on the top of one another has been initially considered; cofacial conformations can be found for instance in discotic liquid crystalline phases.[66,67] In the following, we also report the results of such model calculations for pentacene (even though the crystal structure of pentacene is of herringbone type[55]) since derivatization can lead to cofacial/displaced configurations,[24,25] similar to those investigated here.

Figure 7 displays the evolution of the electronic splittings ($2t$) of HOMO and LUMO levels as a function of the distance between the molecular planes in a cofacial dimer of ADT. The calculated electronic splittings of the anti and syn ADT isomers are nearly identical and are on the order of a few tenths of an eV below an intermolecular distance of 4.0 Å. The HOMO splittings are systematically found to be larger than the LUMO splittings in the range of 3.5–5.0 Å.

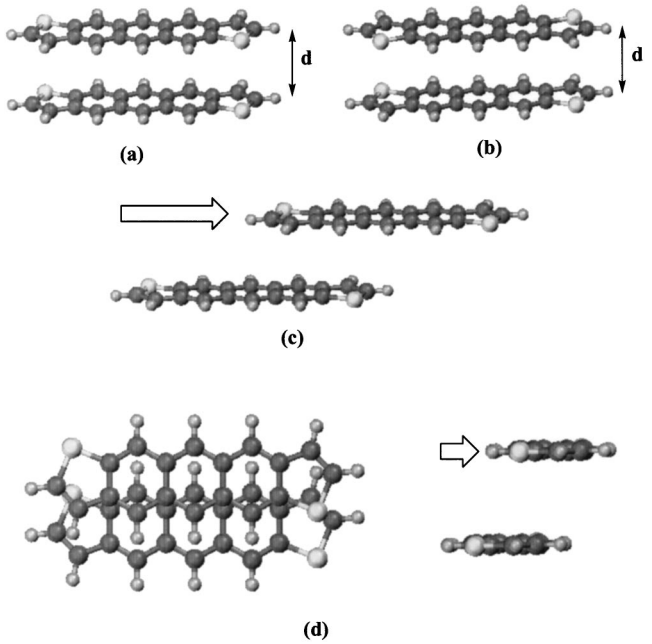

FIG. 6. Displacement patterns in cofacial dimer: (a), (b) separation of dimer as a function of intermolecular distance; (c) lateral displacement along the long molecular axis; (d) lateral displacement along the short molecular axis.

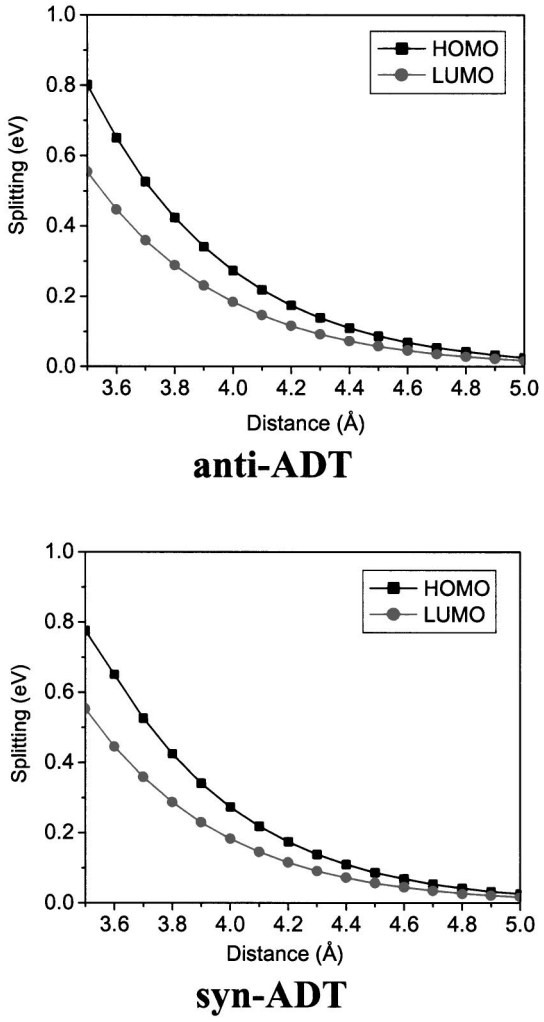

FIG. 7. Evolution of the calculated HOMO and LUMO splittings in a cofacial dimer as a function of the intramolecular distance.

As expected, both decay exponentially as the intermolecular distance is increased; they are reduced by a factor of 3 in going from 3.5 to 4.0 Å, which is a range of intermolecular distances typically encountered in organic conjugated crystals and films.[68,69]

Another dimer configuration in which one molecule is rotated by 180° around its long molecular axis has also been considered. In this case, the molecular planes are still parallel and perfectly superimposed over the central anthracene segment, while the terminal thiophene rings point in opposite directions. For an intermolecular distance of 4.0 Å, the HOMO splittings are calculated to be 0.225 and 0.244 eV for the anti and syn isomers, respectively, and are smaller than the corresponding values (0.274 eV for both anti and syn) in the cofacial dimers. This is related to the fact that the global overlap between the HOMO levels is slightly less favorable for the rotated geometry. In contrast, the LUMO splittings, calculated to be 0.17 eV for both isomers, are nearly equivalent to those in the cofacial dimers (0.18 eV) since the sulfur atoms do not contribute to the LUMO level.

It is well established that packing often involves displacements of adjacent molecules along their long or short molecular axes. Figure 8 shows the evolution of the HOMO and LUMO splittings in dimers of anti ADT and pentacene in which the top molecule is translated along its long or short molecular axis for an intermolecular distance fixed at 4.0 Å. It is important to note that a small displacement can lead not only to a significant change in the amplitude of the transfer integral but can also modify its sign (a feature that was not highlighted in our previous work[22]). Strong oscillations of the electronic splittings are observed for translations along the long molecular axis. The overall attenuation of the oscillation patterns with displacement indicates that the intermolecular orbital overlap is progressively reduced as the degree of translation increases. Interestingly, as described previously,[22] there are translations for which the LUMO splitting is larger than the HOMO splitting (thereby potentially favoring electron mobility over hole mobility). For instance, for a translation of 4.5 Å along the long molecular axis, the HOMO and LUMO splittings are 0.011 and 0.088 eV, respectively, for the anti ADT isomer, and 0.032 and 0.136 eV for pentacene. The calculated evolutions depend on the relative positions of the molecules and the bonding–antibonding pattern of the frontier orbitals in the molecule as shown in Fig. 9. Obviously, the absolute values of the electronic splittings are largest when the global overlap between the π orbitals is maximized and reach zero when there occurs perfect cancellation between bonding and antibonding interchain overlap.

For translations along the short molecular axis, the HOMO splittings show two minima for shifts of about 1.5 and 2.0 Å, while the LUMO splittings decrease gradually as the translation proceeds. These trends can also be explained from Fig. 9. The HOMO wave functions display π orbitals with opposite signs along the short molecular axis, which leads to the appearance of minima throughout the translation.

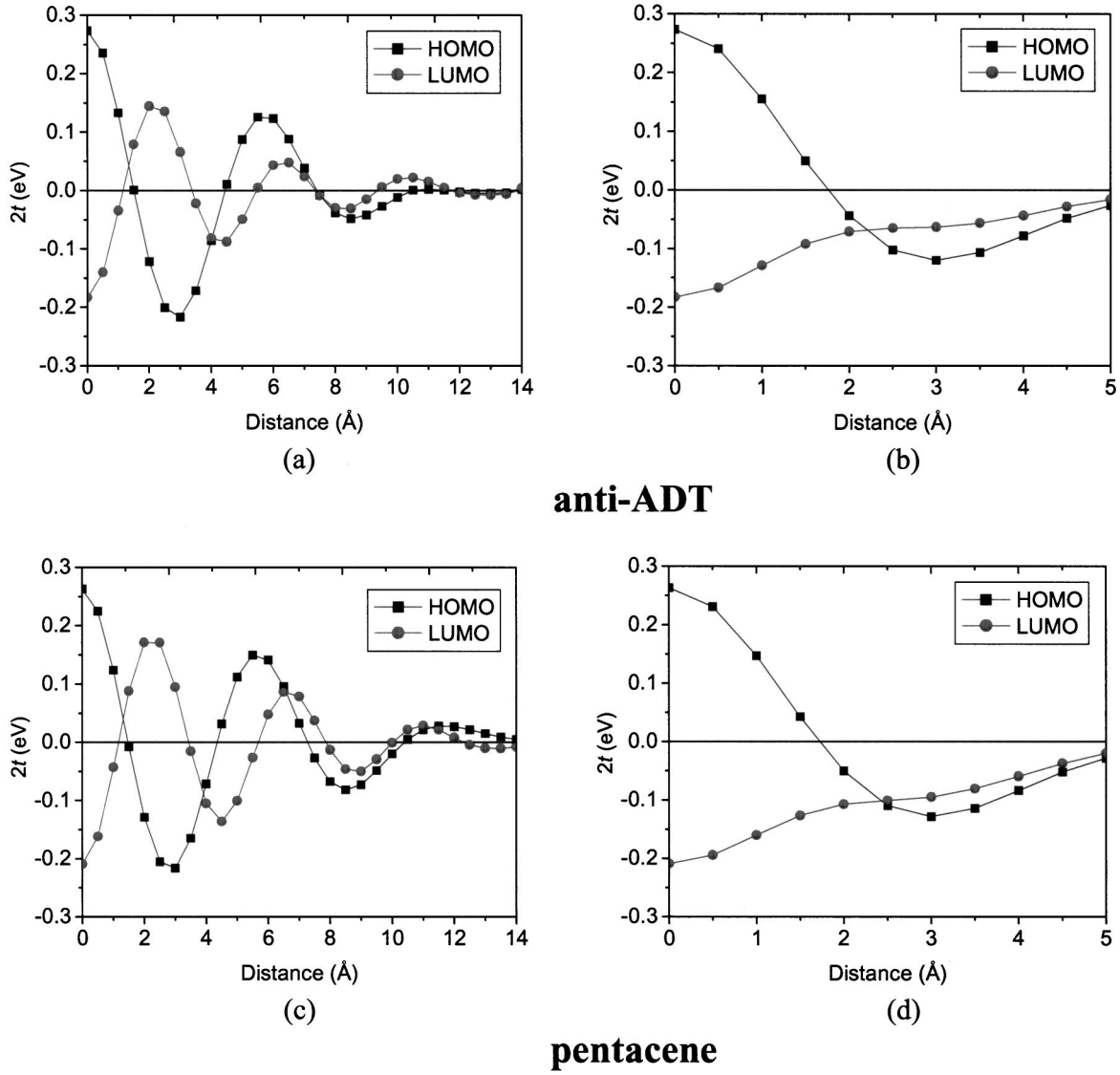

FIG. 8. Evolution of the calculated HOMO and LUMO splittings in a cofacial dimer along the long [(a),(c)] and short [(b),(d)] molecular axes in the ADT and pentacene.

In contrast, the LUMO wave functions do not change sign along the short axis; as a result, the splitting never reaches zero and simply decreases in parallel with the reduction in global overlap.[22] Overall, we can conclude that the influence of the relative positions of adjacent molecules on the HOMO and LUMO splittings is very similar in ADT and pentacene.

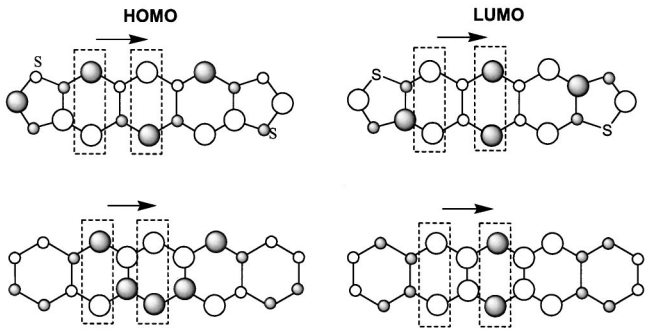

FIG. 9. Illustration of the bonding and antibonding pattern of the HOMO and LUMO in ADT and pentacene. The color and size of the circles represent the sign and amplitude of the orbital coefficients.

Figure 10 shows the evolutions of the total HOMO and LUMO bandwidths formed by the interaction of the HOMO and LUMO levels in clusters containing from one to eight ADT molecules stacked in a perfectly cofacial configuration, with fixed intermolecular distances of 4.0 Å. The results show that the HOMO and LUMO splittings saturate rapidly with cluster size; their evolutions are linear with respect to $\cos[\pi/(N+1)]$, where N is the number of molecules in the stack, as would be expected in the framework of tight-binding models; extrapolating for large N values provides valence and conduction bandwidths for such one-dimensional stacks of ADT molecules of 0.548 and 0.366 eV, respectively; the corresponding values are 0.527 and 0.418 eV for a pentacene stack. Overall, the lower reorganization energies and larger bandwidths for hole than for electron suggest that hole mobility in ADT is expected to be higher

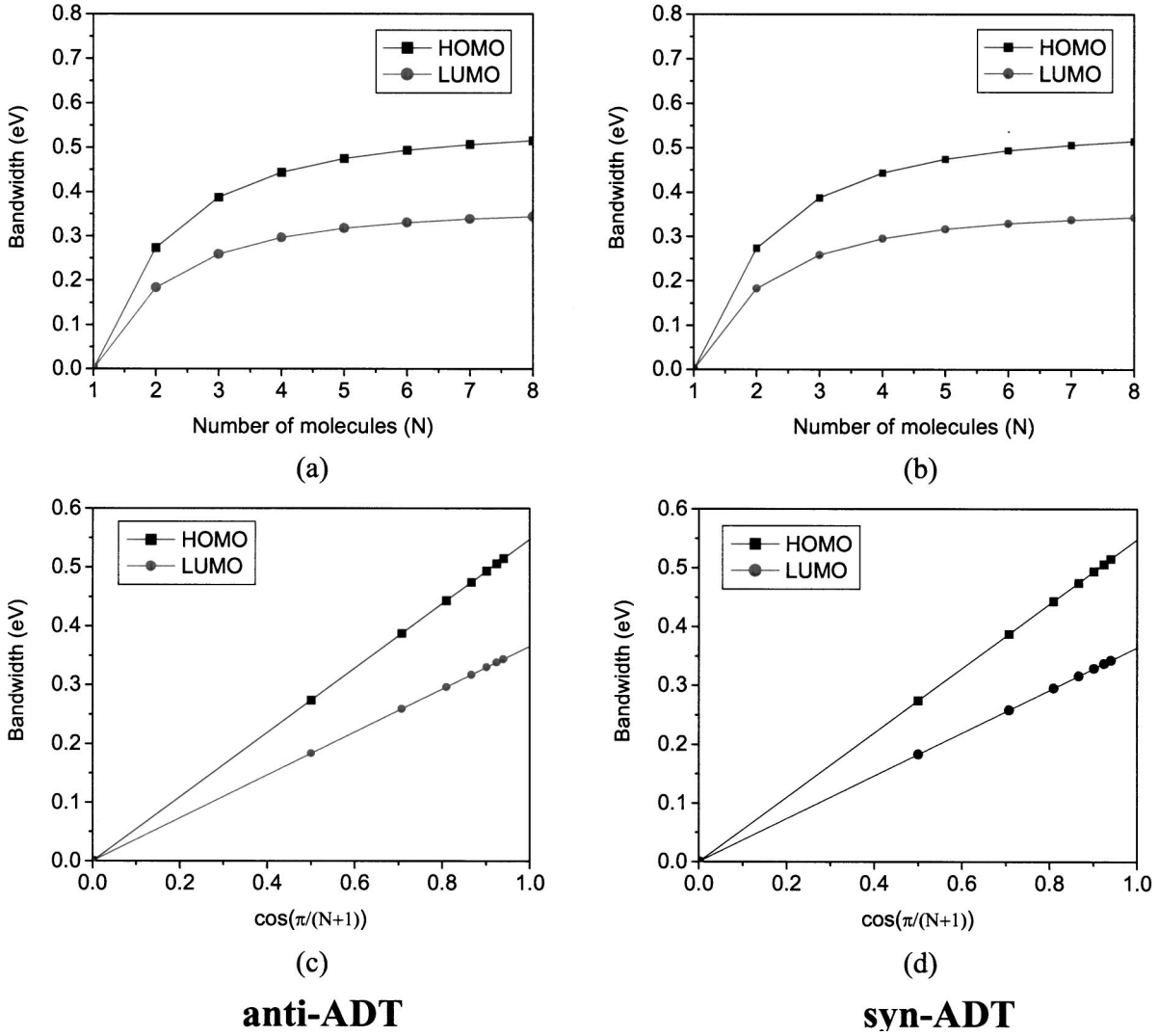

FIG. 10. Evolution of the calculated bandwidths in cofacial clusters separated by 4.0 Å as a function of the number of molecules (N) in a cluster and $\cos[\pi/(N+1)]$.

than electron mobility. This is consistent with the mobility data reported by Katz and co-workers.[30]

Finally, we note that preliminary x-ray-diffraction studies on ADT (Refs. 70 and 71) suggest that the ADT unit cell corresponds to a herringbone packing as in the case of pentacene. Calculations of transfer integrals based on a herringbone-type structure using the same lattice parameters as in pentacene[55] reveal that the HOMO–LUMO splittings in ADT are again very similar to those in pentacene. For instance, the HOMO splitting for holes along the *a* axis (see Ref. 55) is on the order of 0.08 eV for an ADT dimer; that compares very well with the corresponding value of 0.09 eV previously obtained for pentacene.[55]

V. CONCLUSIONS

We have estimated the reorganization energies of positive and negative charge carriers in ADT and found them to be as low as in pentacene. A normal-mode analysis shows that the main contribution to the relaxation energy comes from high-energy vibrations in ADT as well as in pentacene. Despite the fact that the energies of the vibrational modes coupled to the charge-transfer processes lie in the same energy region for both compounds, the actual number of such vibrations is larger in ADT. The nature of the frontier molecular orbitals and vibrational modes are very similar for the two molecules, suggesting that the derivatization of pentacene to form ADT does not change the electronic properties in any significant way. We have also estimated the strength of the transfer integrals by considering dimers in various geometry configurations and cofacial stacks. Again the results are very similar for both ADT and pentacene.

Thus it can be concluded that the molecular parameters governing charge transport are as interesting in ADT as in pentacene, making ADT a promising material for the fabrication of stable and efficient FET's. Additional work to optimize the film deposition parameters and improve the morphology and crystal engineering in ADT could therefore prove very valuable.

ACKNOWLEDGMENTS

The work at Georgia Tech was partly supported by the National Science Foundation, through the STC for Materials

and Devices for Information Technology (Grant No. DMR-0120967) and through Grant Nos. CHE-0343321 and CHE-0078819, the Office of Naval Research and the IBM Shared University Research program. J.C. is a Research Associate of the Belgium National Fund for Scientific Research (FNRS). We thank Theo Siegrist for helpful discussions.

[1] F. Garnier, R. Hajlaoui, A. Yassar, and P. Srivastava, Science **265**, 1684 (1994).
[2] H. E. Katz, J. Mater. Chem. **7**, 369 (1997).
[3] G. Horowitz, Adv. Mater. (Weinheim, Ger.) **10**, 365 (1998).
[4] S. F. Nelson, Y. Y. Lin, D. J. Gundlach, and T. N. Jackson, Appl. Phys. Lett. **72**, 1854 (1998).
[5] H. Sirringhaus, P. J. Brown, R. H. Friend *et al.*, Nature (London) **401**, 685 (1999).
[6] H. E. Katz, A. J. Lovinger, J. Johnson, C. Kloc, T. Siegrist, W. Li, Y. Y. Lin, and A. Dodabalapur, Nature (London) **404**, 478 (2000).
[7] Z. Bao, Adv. Mater. (Weinheim, Ger.) **12**, 227 (2000).
[8] G. H. Gelinck, T. C. T. Geuns, and D. M. de Leeuw, Appl. Phys. Lett. **77**, 1487 (2000).
[9] C. W. Tang and S. A. Van Slyke, Appl. Phys. Lett. **51**, 913 (1987).
[10] J. H. Burroughes, D. D. C. Bradley, A. R. Brown, R. N. Marks, R. H. Friend, P. L. Burn, and A. B. Holmes, Nature (London) **347**, 539 (1990).
[11] J. R. Sheats, H. Antoniadis, M. Hueschen, W. Leonard, J. Miller, R. Moon, D. Roitman, and A. Stocking, Science **273**, 884 (1996).
[12] R. H. Friend, R. W. Gymer, A. B. Holmes *et al.*, Nature (London) **397**, 121 (1999).
[13] N. S. Sariciftci, L. Smilowitz, A. J. Heeger, and F. Wudl, Science **258**, 1474 (1992).
[14] J. J. M. Halls, C. A. Walsh, N. C. Greenham, E. A. Marseglia, R. H. Friend, S. C. Moratti, and A. B. Holmes, Nature (London) **376**, 498 (1995).
[15] G. Yu, J. Wang, J. McElvain, and A. J. Heeger, Adv. Mater. (Weinheim, Ger.) **17**, 1431 (1998).
[16] C. J. Brabec, N. S. Sariciftci, and J. C. Hummelen, Adv. Funct. Mater. **11**, 15 (2001).
[17] Y. Y. Lin, D. J. Gundlach, S. F. Nelson, and T. N. Jackson, IEEE Electron Device Lett. **18**, 606 (1997).
[18] H. Klauk, D. J. Gundlach, J. A. Nichols, and T. N. Jacksons, IEEE Trans. Electron Devices **46**, 1258 (1999).
[19] H. Klauk, K. J. Gundlach, M. Bonse, C. C. Kuo, and T. N. Jackson, Appl. Phys. Lett. **76**, 1692 (2000).
[20] T. W. Kelley, D. V. Muyres, P. F. Baude, T. P. Smith, and T. D. Jones, Mater. Res. Soc. Symp. Proc. **771,** 169 (Materials Research Society, Pittsburgh, 2003).
[21] M. Yamada, I. Ikemote, and H. Kuroda, Bull. Chem. Soc. Jpn. **61**, 1057 (1998).
[22] J. L. Brédas, J. P. Calbert, D. A. da Silva Filho, and J. Cornil, Proc. Natl. Acad. Sci. U.S.A. **99**, 5804 (2002).
[23] P. T. Herwig and K. Müllen, Adv. Mater. (Weinheim, Ger.) **11**, 480 (1999).
[24] J. E. Anthony, J. S. Brooks, D. L. Eaton, and S. R. Parkin, J. Am. Chem. Soc. **123**, 9482 (2001).
[25] J. E. Anthony, D. L. Eaton, and S. R. Parkin, Org. Lett. **4**, 15 (2002).
[26] H. Meng, M. Bendikov, G. Mitchell, R. Helgeson, F. Wudl, Z. Bao, T. Siegrist, C. Kloc, and C. H. Chen, Adv. Mater. (Weinheim, Ger.) **15**, 1090 (2003).
[27] Q. Miao, T. Q. Nguyen, T. Someya, G. B. Blanchet, and C. Nuckolls, J. Am. Chem. Soc. **125**, 10284 (2003).
[28] N. E. Gruhn, D. A. da Silva Filho, T. G. Bill, M. Malagoli, V. Coropceanu, A. Kahn, and J. L. Brédas, J. Am. Chem. Soc. **124**, 7918 (2002).
[29] H. E. Katz and Z. Bao, J. Phys. Chem. B **104**, 671 (2000).
[30] J. G. Laquindanum, H. E. Katz, and A. J. Lovinger, J. Am. Chem. Soc. **120**, 664 (1998).
[31] J. Cornil, N. E. Gruhn, D. A. dos Santos, M. Malagoli, P. A. Lee, S. Barlow, S. Thayumanavan, S. R. Marder, N. R. Armstrong, and J. L. Brédas, J. Phys. Chem. A **105**, 5206 (2001).
[32] V. Coropceanu, M. Malagoli, D. A. da Silva Filho, N. E. Gruhn, T. G. Bill, and J. L. Brédas, Phys. Rev. Lett. **89**, 275503 (2002).
[33] J. Cornil, D. Beljonne, J. P. Calbert, and J. L. Brédas, Adv. Mater. (Weinheim, Ger.) **13**, 1053 (2001).
[34] K. C. Kao and W. Hwang, *Electrical Transport in Solids* (Pergamon, Oxford, 1981).
[35] M. Pope and C. E. Swenberg, *Electronic Processes in Organic Crystals and Polymers*, 2nd Ed. (Oxford University, New York, 1999).
[36] E. A. Silinsh and V. Capek, *Organic Molecular Crystals: Interaction, Localization, and Transport Phenomena* (AIP, New York, 1994).
[37] B. S. Brunschwig, C. Creutz, and N. Sutin, Chem. Soc. Rev. **31**, 168 (2002).
[38] P. F. Barbara, T. J. Meyer, and M. A. Ratner, J. Phys. Chem. **100**, 13148 (1996).
[39] K. D. Demadis, C. M. Hartshorn, and T. J. Meyer, Chem. Rev. **101**, 2655 (2001).
[40] M. Bixon and J. Jortner, *Electron Transfer: From Isolated Molecules to Biomolecules, Adv. Chem. Phys. 106–107* (Wiley, New York, 1999).
[41] M. Malagoli and J. L. Brédas, Chem. Phys. Lett. **327**, 13 (2000).
[42] J. R. Reimers, J. Chem. Phys. **115**, 9103 (2001).
[43] V. Coropceanu, J. M. André, M. Malagoli, and J. L. Brédas, Theor. Chem. Acc. **110**, 59 (2003).
[44] W. Koch and M. C. Holthausen, *A Chemist's Guide to Density Functional Theory* (Wiley, New York, 2000).
[45] R. G. Parr and W. Yang, *Density-Functional Theory of Atoms and Molecules* (Oxford University Press, Oxford, 1989).
[46] A. D. Becke, J. Chem. Phys. **98**, 5648 (1993); C. Lee, W. Yang, and R. G. Parr, Phys. Rev. B **37**, 785 (1988).
[47] R. Ditchfield, W. J. Hehre, and J. A. Pople, J. Chem. Phys. **54**, 724 (1971); W. J. Hehre, R. Ditchfield, and J. A. Pople, *ibid.* **56**, 2257 (1972); P. C. Hariharan and J. A. Pople, Theor. Chim. Acta **28**, 213 (1973); P. C. Hariharan and J. A. Pople, Mol. Phys. **27**, 209 (1974); M. S. Gordon, Chem. Phys. Lett. **76**, 163 (1980).
[48] M. J. Frisch, G. W. Trucks, H. B. Schlegel *et al.*, Gaussian 98, Revision A11, Gaussian, Inc., Pittsburgh, PA, 2001.
[49] M. D. Newton, Chem. Rev. **91**, 767 (1991).
[50] C. J. Calzado and J. P. Malrieu, Chem. Phys. Lett. **317**, 404 (2000).
[51] T. Koopmans, Physica (Amsterdam) **1**, 104 (1933).
[52] J. Ridley and M. C. Zerner, Theor. Chim. Acta **32**, 111 (1973).
[53] M. C. Zerner, G. H. Loew, R. F. Kichner, and U. T. Mueller-Westerhoff, J. Am. Chem. Soc. **102**, 589 (1980).
[54] J. L. Brédas, D. Beljonne, J. Cornil, J. P. Calbert, Z. Shuai, and R. Silbey, Synth. Met. **125**, 107 (2002).
[55] J. Cornil, J. P. Calbert, and J. L. Brédas, J. Am. Chem. Soc. **123**, 1250 (2001).
[56] J. Cornil, J. P. Calbert, D. Beljonne, R. Silbey, and J. L. Brédas, Adv. Mater. (Weinheim, Ger.) **12**, 978 (2000).
[57] M. D. Newton, Int. J. Quantum Chem. **77**, 255 (2000).
[58] P. Rademacher, B. Kettler, K. Kowski, and M. E. Weiß, Spectrochim. Acta, Part A **57**, 2475 (2001).
[59] T. Kato and T. Yamabe, J. Chem. Phys. **115**, 8592 (2001).
[60] T. Kato, K. Yoshizawa, and K. Hirao, J. Chem. Phys. **116**, 3420 (2002).
[61] T. Kato and T. Yamabe, J. Chem. Phys. **118**, 3804 (2003).
[62] F. Duschinsky, Acta Physicochim. URSS **7**, 551 (1937).
[63] Our DFT calculations indicate that the vibrational frequencies of the neutral and cationic states differ only slightly, thus indicating a negligible Duschinsky effect in the ADT molecule.
[64] C. J. Ballhausen, *Molecular Electronic Structures of Transition Metal Complexes* (McGraw-Hill, New York, 1979); P. Chen, *Unimolecular and Bimolecular Ion-Molecule Reaction Dynamics* (Wiley, New York, 1994).
[65] We note that if only the transitions from the vibrational ground state ($m=0$) are considered, the relative intensities of the vibrational transitions [Eq. (5)] are reduced to the standard Poisson distribution.
[66] D. Adam, P. Schuhmacher, J. Simmerer, L. Häussling, K. Siemensmeyer, K. H. Etzbach, H. Ringsdorf, and D. Haarer, Nature (London) **371**, 141 (1994).
[67] A. M. van de Craats, J. M. Warman, A. Fechtenkötter, J. D. Brand, M. A. Harbison, and K. Müllen, Adv. Mater. (Weinheim, Ger.) **11**, 1469 (1999).
[68] X. C. Li, H. Sirringhaus, F. Garnier, A. B. Holmes, S. C. Moratti, N. Feeder, W. Clegg, S. J. Teat, and R. H. Friend, J. Am. Chem. Soc. **120**, 2206 (1998).
[69] R. Goddard, M. W. Haenel, W. C. Herndon, C. Krüger, and M. Zander, J. Am. Chem. Soc. **117**, 30 (1995).
[70] T. Siegrist (private communication).
[71] We considered possible dimers of anti–anti, syn–syn, and anti–syn isomers of ADT; in all cases, the resulting transfer integrals are similar.